Journal of Alloys and Compounds 509 (2011) 9782–9790

Contents lists available at ScienceDirect

Journal of Alloys and Compounds

journal homepage: www.elsevier.com/locate/jallcom

Electrochemical and microstructural study of Cu–Al–Ni shape memory alloy

Mirko Gojić[a,*], Ladislav Vrsalović[b], Stjepan Kožuh[a], Albert Kneissl[c], Ivan Anžel[d], Senka Gudić[b], Borut Kosec[e], Maja Kliškić[b]

[a] University of Zagreb, Faculty of Metallurgy, Aleja narodnih heroja 3, 44103 Sisak, Croatia
[b] Faculty of Chemistry and Technology, Department of Electrochemistry and Materials Protection, Teslina 10/V, 2100 Split, Croatia
[c] Department Metallkunde und Werkstoffprüfung, Montanuniversität Leoben, Franz-Josef-Straße 18, A-8700 Leoben, Austria
[d] University of Maribor, Faculty of Mechanical Engineering, Smetanova ulica 17, 2000 Maribor, Slovenia
[e] University of Ljubljana, Faculty of Natural Sciences and Engineering, Aškerčeva 12, 1000 Ljubljana, Slovenia

ARTICLE INFO

Article history:
Received 22 April 2011
Received in revised form 22 July 2011
Accepted 30 July 2011
Available online 4 August 2011

Keywords:
Shape memory alloys
Corrosion
Electrochemical impedance spectroscopy
Microstructure
Optical microscopy
Scanning electron microscopy

ABSTRACT

The corrosive behaviour of Cu–Al–Ni shape memory alloy in deaerated 0.5 M NaCl solution at 20 °C was studied by means of open circuit potential measurements, linear polarization, potentiodynamic polarization measurements, cyclic voltammetry and electrochemical impedance spectroscopy measurements. The electrode surface was examined by light microscope, SEM, XRD and EDX methods. The polarization measurements have shown that corrosive behaviour of Cu–Al–Ni alloy in NaCl solution was dominated by the Cu component. The results of impedance measurements at open circuit potential have shown that the overall impedance of the system increases with immersion time due to continuous growth of the passive film on the alloy surface. The XRD and EDX analysis showed the presence of copper, aluminium and nickel compounds, Cu-oxides and Cu-chlorides on alloy surface.

1. Introduction

Copper-based alloys have many practical applications because of their good physical properties, high thermal and electrical conductivity, and good corrosion resistance [1–3]. The addition of aluminium to Cu-based alloys increases its corrosion resistance while the presence of nickel is essential in the passivation of Cu–Ni alloys because of its incorporation in the Cu(I) oxide, which is formed on the corroded surface of the alloy.

Cu–Al–Ni alloys belong to a group of functional, smart materials with the property of remembering the shape they had prior to pseudoplastic deformation, called shape memory alloys. Shape memory alloys are a family of metallic alloys with the remarkable ability to switch from one crystallographic structure to another through a change in temperature or applied stress. Such effect of Cu–Al–Ni alloys is based on crystallographic reversible thermoelastic martensitic transformation [4–6]. Generally, these materials can be plastically deformed at low temperatures, and when exposed to higher temperatures they will return to their shape prior to the deformation. Cu–Al–Ni alloys have some considerable advantages over Ni–Ti (such as less difficult melting, casting and composition control, higher Young's modulus, better machinability, better work/cost ratio, and better stability of the two-way shape memory) [7]. Cu–Al–Ni alloy has attracted interest as an alternative to Ni–Ti alloys for some applications. The components of alloy do not oxidize as readily as titanium, they are easy to machine and raw materials are less expensive [8]. Since Cu–Al–Ni alloys do not have biocompatibility of Ni–Ti alloys, they represent a good alternative for non-medical applications.

It is known that the shape memory properties are functions of microstructure, such as grain size, texture and precipitation. The copper based shape memory alloys exhibit on cooling, a martensitic transformation from β-phase to a close packed structure. In the Cu–Al–Ni alloys two types of thermal induced martensites (β'_1 and γ'_1) form depending on alloy composition and heat treatment [9–11].

Owing to the unique properties associated with the shape recovery effect and the material phase changes, shape memory alloys have very diverse application, ranging from everyday consumer product to biomedical implants and space applications. The main use of Cu-shape memory alloys is in actuator and sensor applications [12,13]. There are numerous publications concerning the mechanical properties of Cu-shape memory alloys, but the electrochemical studies of these alloys are scarce.

* Corresponding author. Tel.: +385 44 533 381; fax: +385 44 533 378.
E-mail address: gojic@simet.hr (M. Gojić).

0925-8388/$ – see front matter © 2011 Elsevier B.V. All rights reserved.
doi:10.1016/j.jallcom.2011.07.107

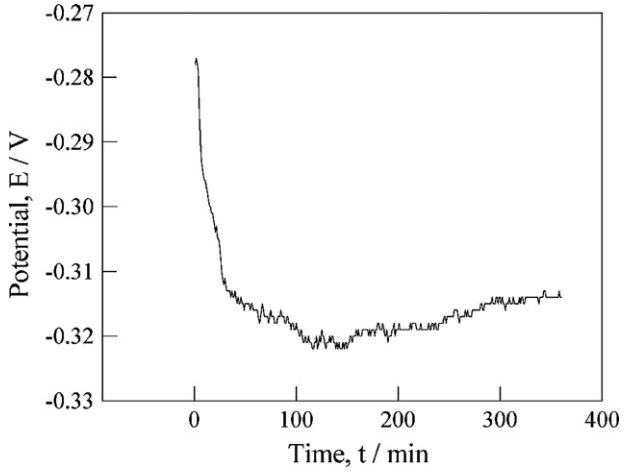

Fig. 1. Open circuit potential vs. time curve for Cu–Al–Ni alloy in deaerated 0.5 M NaCl solution.

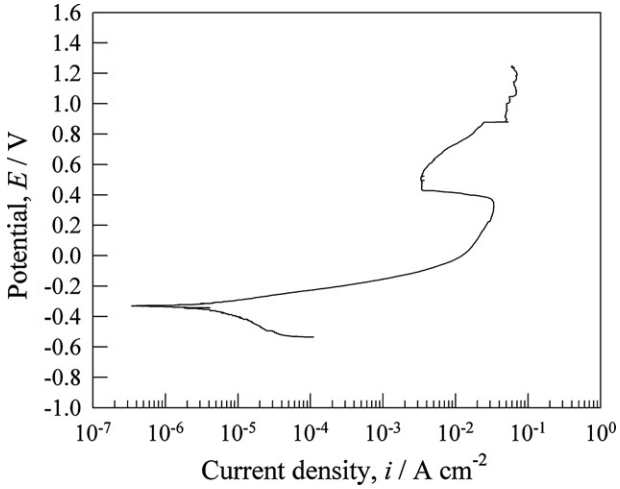

Fig. 2. Potentiodynamic polarization curve for Cu–Al–Ni alloy in deaerated 0.5 M NaCl solution.

The present paper represents a study on the electrochemical behaviour of Cu–Al–Ni alloy in sodium chloride solution and its microstructural analysis, in hope to clarify the mechanism of corrosion processes taking place in a corrosive environment containing chloride ions.

2. Experimental

The Cu–Al–Ni shape memory alloy for investigations was made by melting copper, nickel and aluminium plates in the induction vacuum furnace. The weight of the charge was 15 kg and the heat temperature was 1230 °C. Casting of the heat was carried out on the device for vertical continuous casting at different speed. Cu–Al–Ni alloy for corrosion testing was produced by a casting speed of 335 mm/min and on 2.3–4.5 m of rods. The samples for corrosion testing were cut from a cylindrical rod with 16 mm diameter.

Average chemical composition of investigated Cu–Al–Ni alloy (wt%) was 83.04% Cu, 12.62% Al and 4.34% Ni.

The electrochemical studies were carried out in a conventional three electrode cell with the double-jacket device allowing thermostatic experiments to be performed. The counter electrode was a platinum sheet and the reference electrode was a saturated calomel electrode (SCE) in contact with the working electrode via Luggin capillary. All experiments were performed in a cell containing 250 cm^3 0.5 M NaCl at 20 °C. In order to achieve reproducibility, each experiment was repeated three times.

The working electrodes were prepared by machining the samples of Cu–Al–Ni alloy into cylinders and embedding them in Teflon holders to expose a circular disc (area = 0.502 cm^2) to the electrolyte.

Before each experiment, the working electrode was mechanically polished with different grit emery papers, degreased in acetone, rinsed with double distilled water and immersed in the test solution. In order to perform tests in a deaerated solution, argon was bubbled through the solution 30 min prior to the electrode insertion into the solution, as well as during the experiments. All electrochemical experiments were performed using potentiostat/galvanostat PAR M 273A. The electrochemical methods employed were open circuit potential measurements, linear polarization, potentiodynamic polarization and cyclic voltammetry measurements and electrochemical impedance spectroscopy. Linear polarization measurements were performed in the potential region of ±15 mV around corrosion potential, with the scanning rate of 0.2 mV s^{-1}. Potentiodynamic polarization measurements were performed in the potential region of −0.250 V from open circuit potential to 1.250 V. Cyclic voltammograms were obtained in the −1.2 to 1.4 V potential ranges with the sweep rate of 50 mV s^{-1}. The electrochemical impedance investigations were performed using the PAR M5210 lock-in amplifier. The a.c. amplitude was ±10 mV and the frequency range was from 50 kHz to 10 mHz.

For better understanding of the corrosive behaviour of Cu–Al–Ni alloys in NaCl solution, the morphologies of electrode surfaces after electrochemical testing were analysed. The phase identification was performed by applying the X-ray diffraction (XRD) method using the characteristic CuK_α radiation. XRD testing was carried out using the PHILIPS diffractometer type PW1710 at a current of 30 mA and voltage of 40 kV. Before and after the electrochemical testing selected samples were investigated under light microscope (LM) and scanning electron microscope (SEM) equipped with energy dispersive spectrometer (EDX).

Table 1
Corrosion parameters from polarization measurements.

i_{cor} (μA cm^{-2})	E_{cor} (V)	b_c (V dek^{-1})	b_a (V dek^{-1})	R_p/kΩ cm^{-2}
2.75	−0.329	0.1325	0.06542	4.923

3. Results and discussion

3.1. Open circuit potential measurements

The open circuit potential of the Cu–Al–Ni alloy was traced over the period of 360 min of the electrode immersion in the electrolyte and the results are presented in the Fig. 1.

Following the initial potential decay, a steady state was reached after 1 h from immersion, with a final reading of about −0.315 V. The decrease of E_{OCP} can be explained with the adsorption of the chloride ions and breakdown of the protective surface oxide film [14–16], which could lead to the selective leaching of the active components from the electrode surface [15,16].

3.2. Potentiodynamic and linear polarization measurements

The potentiodynamic polarization behaviour of the alloy in 0.5 M NaCl solution is presented in Fig. 2.

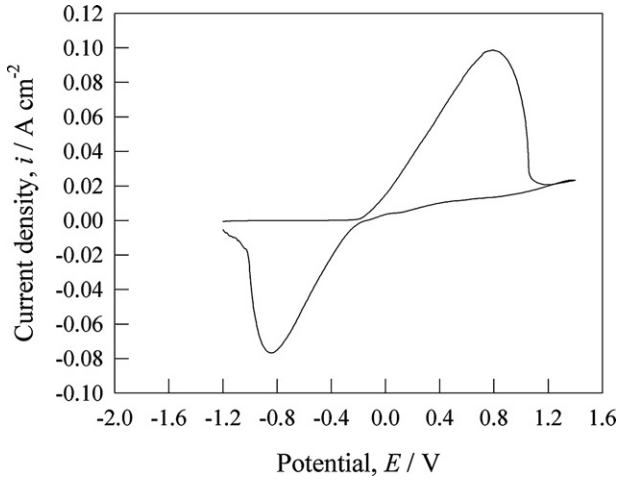

Fig. 3. Cyclic voltammogram for Cu–Al–Ni alloy in deaerated NaCl solution.

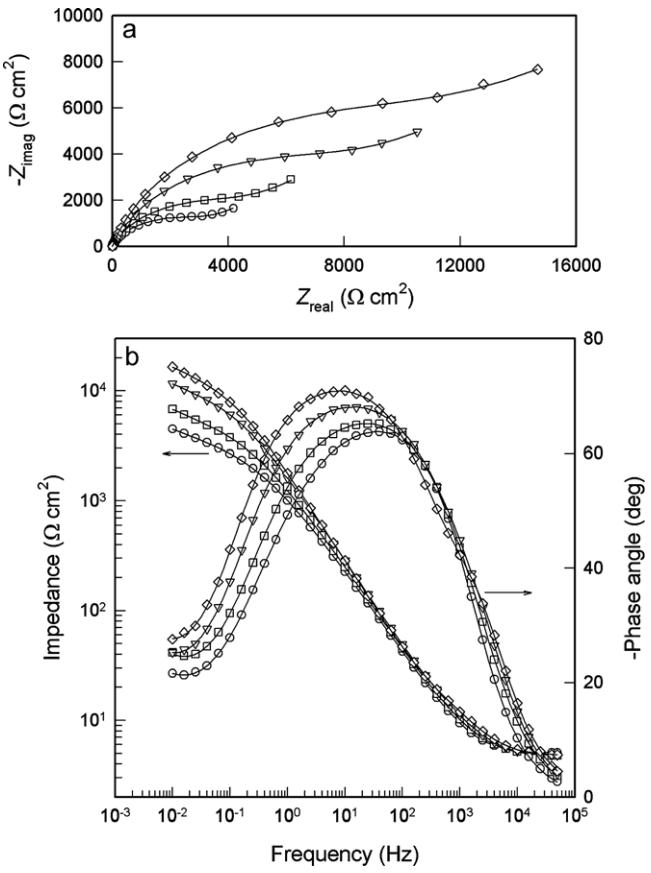

Fig. 4. Nyquist (a) and Bode (b) plots for Cu–Al–Ni alloy exposed to 0.5 M NaCl solution at different exposure times: (○) 1 h, (□) 8 h, (▽) 24 h and (◊) 66 h.

The cathodic branch of the polarization curve represents hydrogen evolution while the anodic branch shows alloy dissolution. Anodic branch of the polarization curve can be divided into three regions: the apparent Tafel region, a region where there is a tendency of the electrode to passivate and the third region in which the current density rises again with the positive potential changes. This anodic behaviour is characteristic for dissolution of copper and its alloys in chloride solutions [17–20]. In the Tafel-type active region, anodic slope was around 60 mV/decade which indicates that the polarization behaviour of this alloy was determinated by the dissolution of copper to soluble cuprous chloride ion complex ($CuCl_2^-$) and its diffusion to the bulk solution [14,16,17]. At more positive potentials, the current density decreases to some extent due to formation of the corrosion products on the electrode surface, which have some protective effect and reduce the active dissolution of metals from the surface. According to the literature, this decrease in current density is usually explained by formation of cuprous chloride (CuCl) and cuprous oxide (Cu_2O), surface adsorbed precipitates [16,19,21], but it can be also the result of formation of aluminium oxide/hydroxide layer, which has been found in the similar corrosion investigation on the surface of Cu–Al and Cu–Al–Ag alloys in 0.5 mol dm^{-3} NaCl solution [17]. In this case, EDX analysis revealed the presence of relatively high amount of Al on the surface which can be indication of aluminium oxide, hydroxide or oxychloride surface layers formation (details in Section 3.5). Increasing the potential, the current density begins to rise again indicating that the formed surface layers do not represent real protective film and the copper dissolution continues. In this region, the increase in current density is due to the formation of Cu(II) species [19]. Table 1 shows the corrosion parameters from potentiodynamic polarization measurements as well as the value of polarization resistance obtained from linear polarization measurement.

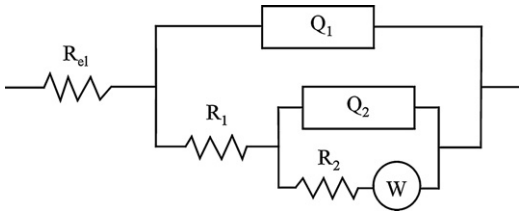

Fig. 5. Proposed equivalent circuit for Cu–Al–Ni alloy in 0.5 M NaCl solution.

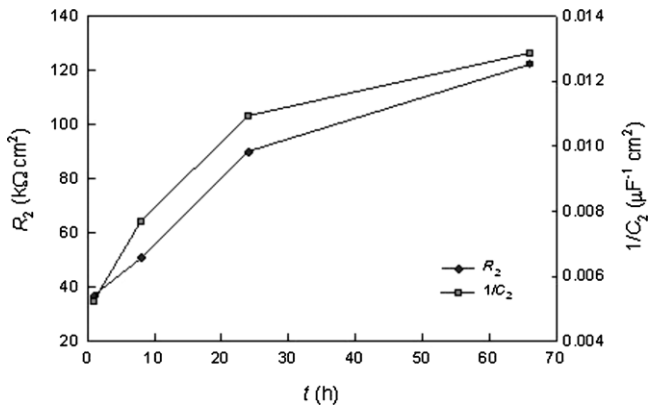

Fig. 6. Variation of the surface film resistance, R_2, and the surface layer thickness, $1/C_2$ of the Cu–Al–Ni alloy as function of immersion time in the 0.5 M NaCl solution.

3.3. Cyclic polarization measurements

Fig. 3 shows the cyclic voltammogram curve for Cu–Al–Ni alloy obtained by cyclic scanning in the potential range between −1.2 and 1.4 V with a scan rate of 50 mV s^{-1}.

The CV curve can be characterized with one anodic current density peak and cathodic current density peak. Literature data show that cyclic voltammograms for copper and copper alloys often have two anodic peaks [17,22]. The existence of the first peak is then related to the formation of CuCl layer on the metal surface. The breakdown of this film by the complexation–dissolution and copper oxidation results in the second peak. In this case the existence of only one anodic peak can be explained by the formation

Fig. 7. Optical micrograph of Cu–Al–Ni shape memory alloy before electrochemical testing.

Table 2
Equivalent circuit parameters for the Cu–Al–Ni alloy in 0.5 M NaCl solution at various immersion times.

t (h)	$Q_1 \times 10^6$ (Ω^{-1} s^n cm^{-2})	n_1	C_1 ($\mu F\,cm^{-2}$)	R_1 ($\Omega\,cm^2$)	$Q_2 \times 10^6$ (Ω^{-1} s^n cm^{-2})	n_2	C_2 ($\mu F\,cm^{-2}$)	R_2 ($k\Omega\,cm^2$)	$W \times 10^3$ (Ω^{-1} s^n cm^{-2})
1	54.12	0.89	22.58	15.67	191.03	0.61	152.49	3.68	2.13
8	58.57	0.86	18.53	14.51	129.92	0.66	104.78	5.07	1.18
24	47.11	0.87	16.64	20.04	91.65	0.72	85.00	8.99	0.74
66	40.97	0.87	14.13	19.68	77.69	0.79	76.62	12.22	0.48

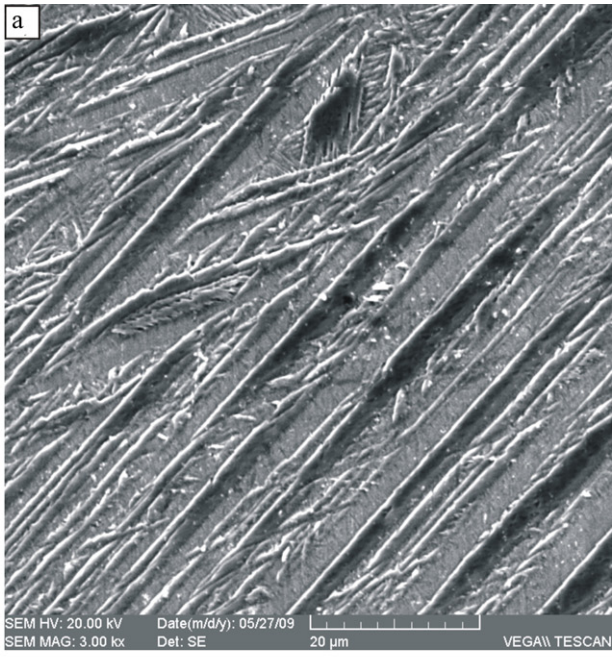

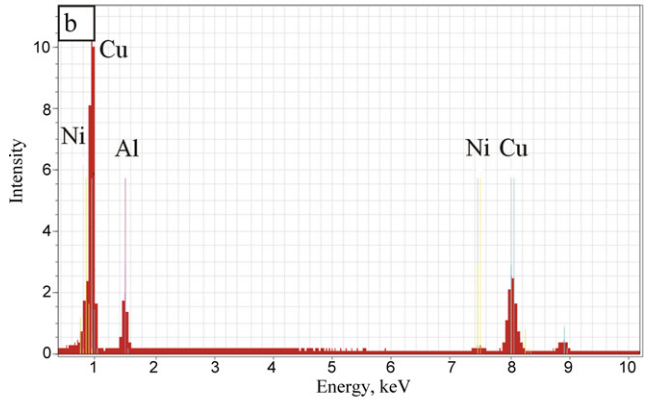

Spectrum: matrix1

El	AN	Series	unn. C [wt.%]	norm. C [wt.%]	Atom. C [at .%]	Error [%]
Cu	29	K-series	82.21	82.90	70.32	2.3
Al	13	K-series	12.84	12.95	25.87	0.7
Ni	28	K-series	4.12	4.16	3.82	0.2
Total:			99.18	100 .00	100.00	

Fig. 8. SEM micrograph (a) and EDX results (b) of Cu–Al–Ni alloy before electrochemical testing.

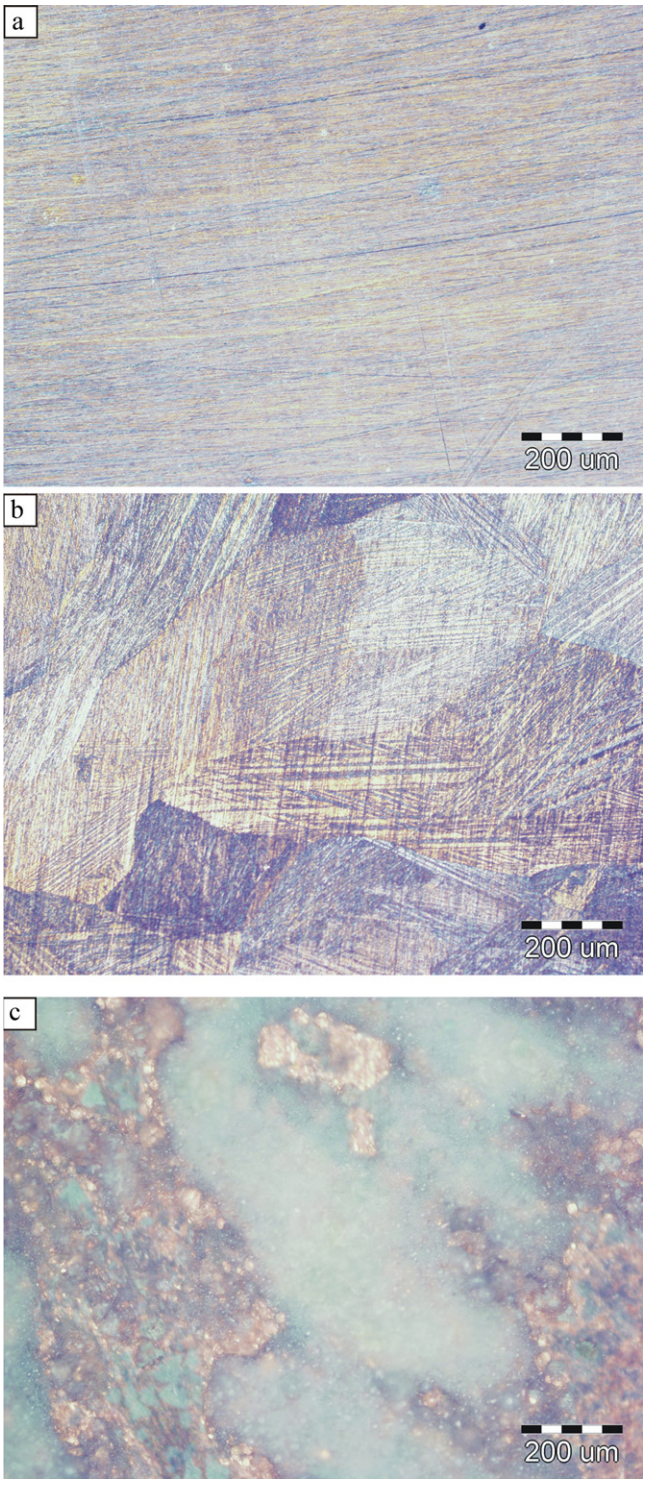

Fig. 9. Optical micrographs of surface morphology of Cu–Al–Ni shape memory alloy after electrochemical testing: (a) specimen 1, (b) specimen 2 and (c) specimen 3.

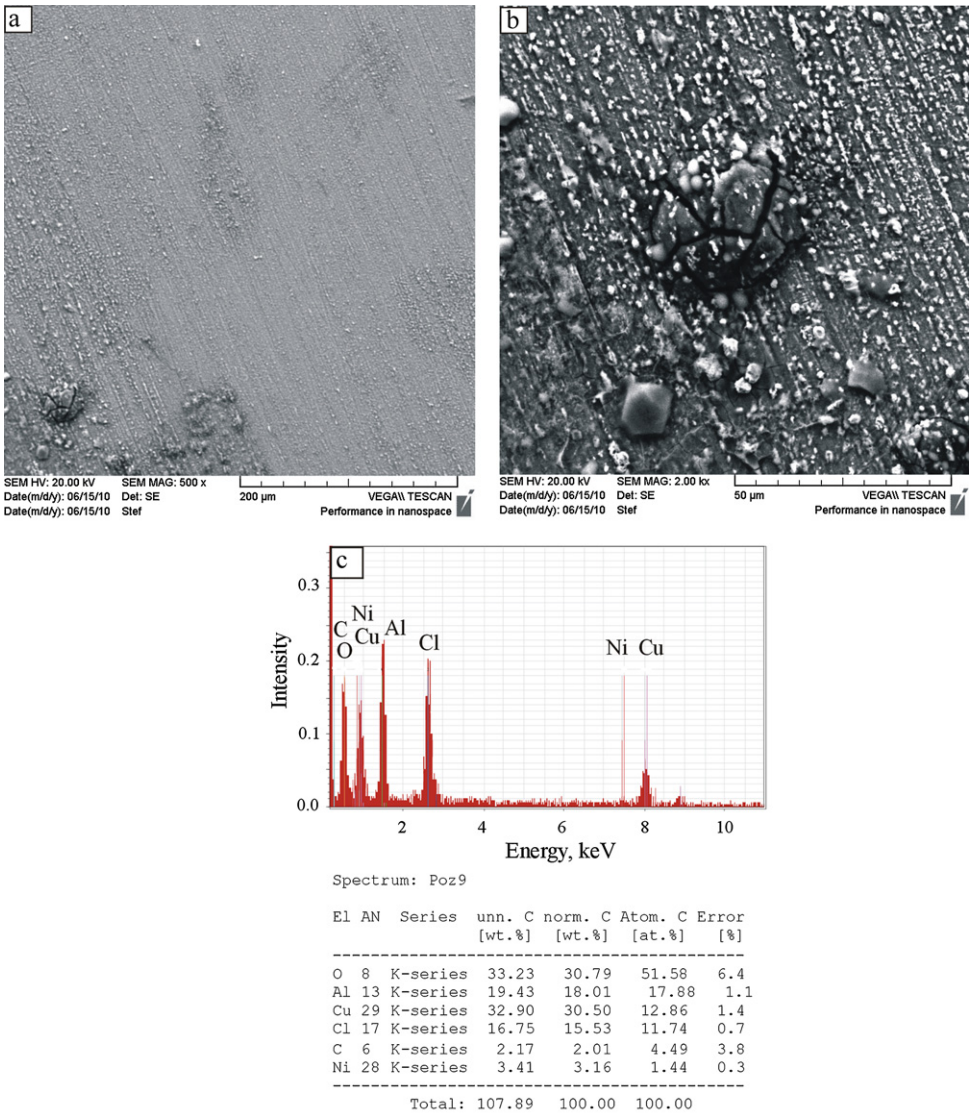

Spectrum: Poz9

El	AN	Series	unn. C [wt.%]	norm. C [wt.%]	Atom. C [at.%]	Error [%]
O	8	K-series	33.23	30.79	51.58	6.4
Al	13	K-series	19.43	18.01	17.88	1.1
Cu	29	K-series	32.90	30.50	12.86	1.4
Cl	17	K-series	16.75	15.53	11.74	0.7
C	6	K-series	2.17	2.01	4.49	3.8
Ni	28	K-series	3.41	3.16	1.44	0.3
		Total:	107.89	100.00	100.00	

Fig. 10. SEM images of the Cu–Al–Ni alloy surface (a and b) and EDX results of corrosion products (c) for specimen 1.

of aluminium hydroxide/oxide layer along with the CuCl surface layer [17]. The aluminium hydroxide layer increases the difficulty of copper–chloride reaction on the surface and so shifts it to higher potentials. In this case the first peak is inhibited by the presence of aluminium hydroxide/oxide and that is the reason for the existence of only one anodic peak in the CV diagram. A large cathodic peak represents electroreduction of the soluble copper species and the CuCl and possible Cu_2O surface layers [17,22,23].

3.4. Impedance measurements

In order to obtain a physical image of the system that is being observed and in order to explain all processes at the Cu–Al–Ni/NaCl phase boundary, impedance measurements have been performed at different stabilisation times at open circuit potential. The results of the impedance measurements are presented in Fig. 4 in the form of Nyquist and Bode plots.

The response of the system in the Nyquist complex plane (Fig. 4a) consists of two more or less poorly separated time constants. The each time constant increased with the increase in stabilization time.

A more convenient method, which better shows the frequency dependence of the impedance data, is the so-called Bode diagram representation (Fig. 4b). At high frequencies ($f > 1$ kHz) the data are dominated by electrolyte resistance. In the medium frequency region, the linear $\log|Z|$ vs. $\log f$ relationship with slope close to -1 and the phase angle of $\approx -70^\circ$ determined the capacitive behaviour of the system. At the lowest frequencies, the phase angle of $\approx -25^\circ$ and slope of $\log|Z|$ vs. $\log f$ close to -0.5 pointed out the presence of a slow diffusion process. It can be seen that the overall impedance of the system increases with immersing time, which indicates that the electrode surface gets more protection.

The development of more than one time constant is deduced from the inspection of the spectra, which reflect the diversity of the phenomena, which occurs in the system under investigation.

The equivalent circuit proposed to fit the experimental data is shown in Fig. 5. It consists of electrolyte resistance R_{el} ($\approx 5\,\Omega\,cm^2$) connected with two time constants. The model is based on the circuits mostly used in the literature for simulation of the kinetics of alloy corrosion process and the protective properties of surface corrosion product layer [15,24–28].

The first time constant, observed in the high frequency region, is the result of the fast charge transfer process in the alloy dissolution reaction in the NaCl solution. In this case, R_1 represents the charge transfer resistance, and Q_1 represents the constant phase element and replaces the capacitance of the electrochemical double layer.

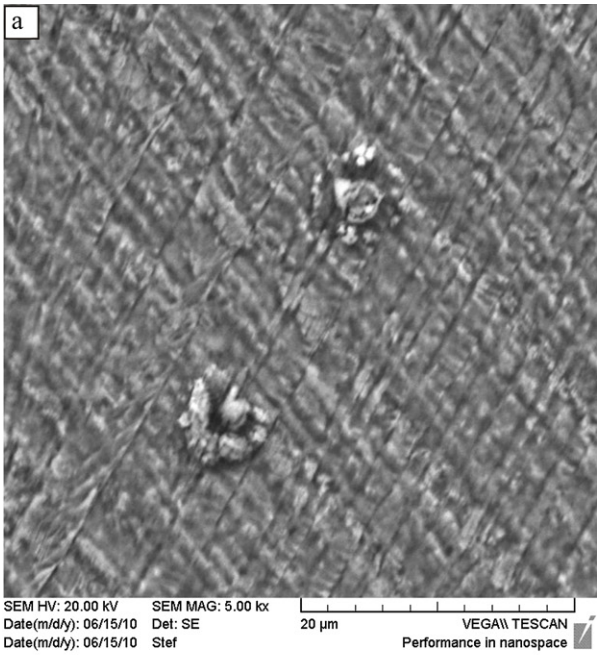

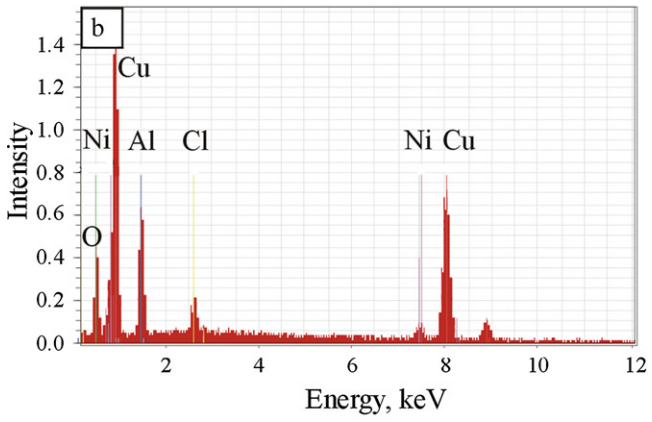

Spectrum: Poz4

El	AN	Series	unn. C [wt.%]	norm. C [wt.%]	Atom. C [at.%]	Error [%]
Cu	29	K-series	71.04	67.87	43.47	2.1
O	8	K-series	13.26	12.67	32.22	2.2
Al	13	K-series	12.35	11.80	17.80	0.7
Ni	28	K-series	5.26	5.03	3.49	0.2
Cl	17	K-series	2.76	2.64	3.03	0.1
		Total:	104.66	100.00	100.00	

Fig. 11. SEM micrography of Cu–Al–Ni alloy surface (a) and EDX results of corrosion products (b) for specimen 2.

To account for the surface layer and diffusion process in the low frequency range, additional equivalent circuit parameters were introduced, such as R_2 for the surface layer resistance, Q_2 for constant phase element of the surface layer (Q_2 replaces the capacitance of surface layer) and Warburg impedance (W) for diffusion process. The presence of the diffusion process within the interfacial layer indicates a reversible dissolution in which surface film formation under open circuit condition proceeds through a dissolution–precipitation (re-deposition) mechanism [29].

As can be seen, the constant phase elements (CPEs) replace the capacitive elements in the proposed equivalent circuit. In many

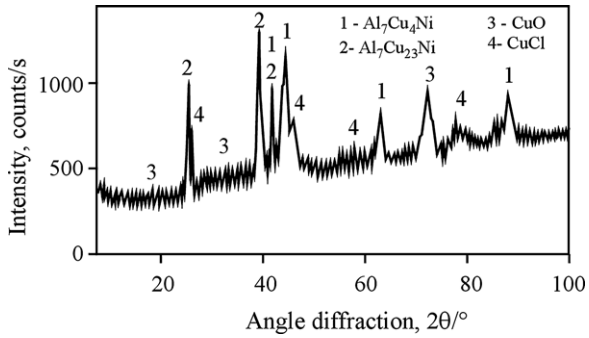

Fig. 12. X-ray diffraction spectrum of Cu–Al–Ni alloy after electrochemical testing.

cases CPE is used to describe the distribution of relaxation times, as a result of inhomogeneities present at the solid/liquid interface on a microscopic level (like surface inhomogeneity, roughness, adsorption, formation of porous layers, and variation in properties or compositions of surface layer) [30–36]. Its impedance, Z_{CPE}, is described by expression (1) [30]:

$$Z_{CPE} = [Q(j\omega)^n]^{-1} \quad (1)$$

with $-1 \le n \le 1$, $j = \sqrt{-1}$ and $\omega = 2\pi f$, while Q is a frequency independent constant, being defined as pure capacitance for $n = 1$, resistance for $n = 0$, inductance for $n = -1$. Diffusion processes are characterized by the value of $n = 0.5$.

The calculated equivalent circuit parameters for the Cu–Al–Ni alloy in chloride solution at different immersion times are presented in Table 2.

The capacitance was calculated from Q using the equation [37]:

$$C = [QR^{1-n}]^{1/n} \quad (2)$$

The values of the electrochemical double layer capacitance (C_1) and the film capacitance (C_2) are also presented in Table 2. The capacitance of the electrical double layer is proportional to the corrosion rate. Also, the smaller the charge transfer resistance, the faster the corrosion rate. As shown in Table 2, it is clear that the corrosion rate of the alloy decreases with the immersion time up to 66 h.

Furthermore, the obtained results indicate that the surface layer resistance (R_2) increased, while the capacitance of the surface layer (C_2) and the diffusion element (W) decreases with immersion time up to 66 h. This direction of the change is attributed to the increase of protective properties of the surface layer on the electrode. According to the plate capacitor model the oxide film capacitance, C, is inversely proportional to its thickness, d:

$$C = \frac{\varepsilon_o \varepsilon}{d} \quad (3)$$

where ε_o is the permittivity of vacuum, ε is the dielectric constant of the surface film.

Although the actual value of the dielectric constant of the surface film is difficult to estimate (since the EDX analysis shows that the surface layer consists of Cu, Al, Ni, O and Cl, which is discussed in detail in Section 3.5) a change of C_2 can be used as an indicator of a change in the film thickness. Assuming that the dielectric constant does not change with the different parameters under investigation, the reciprocal capacitance of surface film, $1/C_2$, will be directly proportional to the thickness of the film. The thickness and the resistance of the surface film increase with the increase of the time immersion (Fig. 6), thus indicating a continuous growth of the passive film on the alloy surface. Furthermore, the values of n_2 for the Cu–Al–Ni alloy also increase with time, indicating a possible increase in surface homogeneities. This additionally pointed to the increase of protective properties of the surface layer.

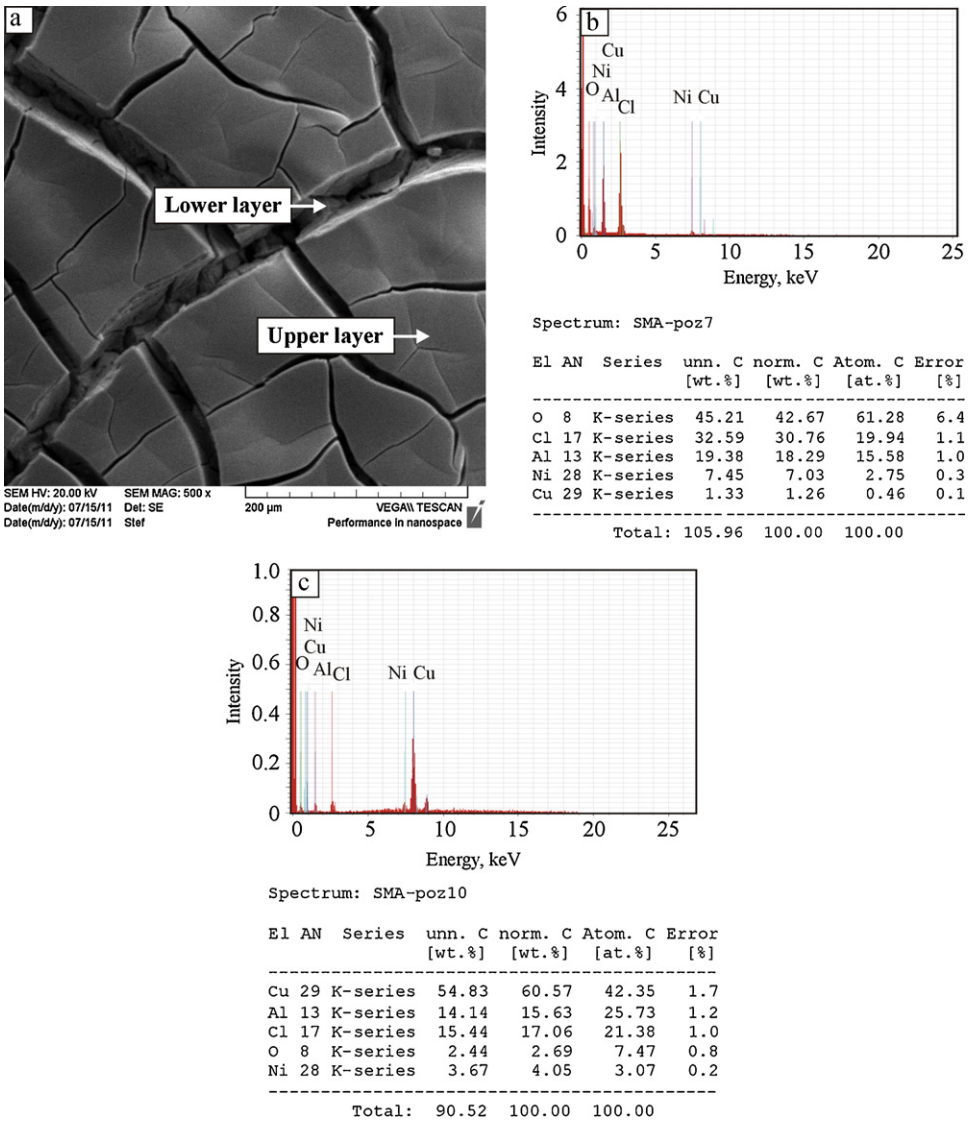

Fig. 13. (a) SEM image of Cu–Al–Ni alloy surface after potentiodynamic polarization measurement which was interrupted at 0.4 V. (b) Results of EDX analysis for the upper layer of corrosion products. (c) Results of EDX analysis for the lower layer of corrosion products.

3.5. Microstructure and surface analysis

The surface of the electrodes before electrochemical experiments was examined with light microscope, SEM and EDX analysis and the results are presented in Figs. 7 and 8.

As can be seen from optical and scanning electron micrographs of the Cu–Al–Ni alloy (Figs. 7 and 8) the microstructure includes grains with martensite plates. The parallel bands in martensite can be considered twin-like martensite, which is confirmed by SEM micrographs (Fig. 8). The chemical composition of the investigated alloy was obtained using EDX analysis (Fig. 8b).

Also, after corrosion testing, surface morphologies of the three selected specimens were investigated with light microscopy, scanning electron microscopy and energy dispersive X-ray spectroscopy. Three selected specimens were marked with:

- specimen 1: Cu–Al–Ni alloy, 24 h immersion in deaerated 0.5 mol dm^{-3} NaCl solution at E_{OC};
- specimen 2: Cu–Al–Ni alloy after a potential hold at −0.2 V;
- specimen 3: Cu–Al–Ni alloy after potentiodynamic polarization measurement which was interrupted at 0.4 V.

As shown in Fig. 9 typical martensite microstructure can be seen only on the surface on specimen 2. Other observed microstructures demonstrated the occurrence of corrosion products on the surface of Cu–Al–Ni alloy after 24 h immersion and after polarization testing. As can be seen from micrographs the microstructure includes grains and martensite plates (Fig. 9). The grains appear clearly and martensite plates have different orientations within particular grains. As is well known, martensite is formed primarily as the needle-like shape and β martensite is the typical morphology for Cu–Al–Ni shape memory alloys [37].

In this work the SEM and EDX analyses were used to characterize the morphology of Cu–Al–Ni alloy after an electrochemical study. Also, the EDX analysis was used to show the chemical composition of corrosion products (surface attack) which were formed on the surface of the specimen after corrosion testing. Typical SEM micrographies for the localized attack are shown in Fig. 10a and b. The EDX analyses of Cu–Al–Ni alloy after impedance measurement 24 h

in deaerated 0.5 M NaCl at E_{OC} revealed (depending on the place of analysis) the presence of 10–30% oxygen, 17–70% copper, 11–34% Al, 2–6% nickel and 2–15% chlorine (wt%) (Fig. 11c).

The relatively high percentage of oxygen on the alloy surface can be explained by the formation of Cu_2O and $Al(OH)_3$ layers on the electrode surface [17,20,22]. By investigating the corrosion behaviour of pure Cu and Cu-alloys in solutions containing Cl^- ions, it was established that at least two different corrosion products can be found at the electrode surface, i.e. CuCl and Cu_2O [17,20,22,38]. The CuCl surface layer formed rapidly on the electrode surface, while the Cu_2O layer formed after a longer immersion period by hydrolysis of CuCl [20,22,38]. As this analysis was performed after the 24 h immersion period, probably the large quantities of CuCl was hydrolysed to Cu_2O, and that is the reason for the relatively high percentage of oxygen and lower percentage of Cl on electrode surface.

After interruption of electrochemical testing at different times and potentials, variation in surface morphology and compositions of corrosion products were observed (Fig. 11). Thus, the EDX analysis showed that corrosion products at the surface of Cu–Al–Ni alloy, after submitting the electrode surface to potential of −0.2 V, were: 2–16% oxygen, 65–80% copper, 6–12% aluminium, 2–5% nickel and 1–5% chlorine (wt%).

It is likely that the corrosion products consist mainly of copper chloride and copper oxide, along with aluminium hydroxide and nickel incorporated in these copper oxide/chloride surface layers [17,20,27].

Fig. 12 shows XRD spectra of Cu–Al–Ni alloy after corrosion testing. Besides the Al_7Cu_4Ni and $Al_7Cu_{23}Ni$ compounds, the peaks of the diffraction pattern were indexed to be CuO and CuCl compounds.

The greatest differences in results of EDX analysis for corrosion products were observed for Cu–Al–Ni alloy after potentiodynamic polarization which was interrupted at 0.4 V. After potentiodynamic polarization measurement two layers of corrosion products on the Cu–Al–Ni surface were observed (Fig. 13a). The upper layer of corrosion products consisted of: 42.7% oxygen, 18.3% aluminium, 7.0% nickel and 30.8% chlorine (wt%) (Fig. 13b). In contrast, the lower layer of corrosion products consisted of: 2.7% oxygen, 60.6% copper, 15.6% aluminium, 4.1% nickel and 17.1% chlorine (wt%) (Fig. 13c).

It seems that the upper layer of corrosion products consists mainly of aluminium and nickel oxides and probably aluminium hydroxides and oxychloride complexes, while the inner layer also contains copper, probably in the form of chloride or oxide. In their corrosion research of Cu–Al–Ag alloy in NaCl solution, Benedetti et al. [17] have found that the exposure of electrodes to positive potentials leads to the formation of a surface layer of hydrated aluminium oxide/hydroxide which completely covers the CuCl layer, and this could explain the lack of copper in the upper layer of corrosion products.

4. Conclusions

The corrosion behaviour of Cu–Al–Ni shape memory alloy in 0.5 M NaCl solution was investigated by linear and potentiodynamic polarization, cyclic voltammetry and electrochemical impedance spectroscopy. The results of corrosion testing and microstructure analysing suggest the following conclusions:

- The results of open circuit potential measurements for Cu–Al–Ni alloy in 0.5 M NaCl solution have shown that the adsorption of chloride ions on the electrode surface leads to the decrease of E_{OCP} values and the breakdown of the protective surface oxide film.
- In the potentiodynamic polarization curve (Tafel-type active region) the anodic slope was around 65 mV/decade, which indicates that the polarization behaviour of this alloy was determinated by the dissolution of copper to soluble cuprous chloride ion complex ($CuCl_2^-$) and its diffusion to the bulk solution. At more positive potentials the current density decreases to some extent due to the formation of corrosion products on the electrode surface, which have some protective effect and reduce the active dissolution.
- The CV curve can be characterized by one anodic current density peak and the cathodic current density peak. The existence of one anodic peak can be explained by the formation of aluminium hydroxide/oxide layer along with the CuCl surface layer. A large cathodic peak represents electroreduction of the soluble copper species and the CuCl and possible Cu_2O surface layers.
- The results of the impedance measurements, performed at different stabilization times at open circuit potential, have shown that the overall impedance of the system increases with immersing time due to continuous growth of the passive film on the alloy surface.
- Optical and scanning electron microscopy analysis prior to electrochemical testing showed the presence of grains with martensite plates in microstructure.
- Microstructures after corrosion testing demonstrated the occurrence of corrosion products at surface of Cu–Al–Ni alloy. The EDX analyses revealed the presence of copper, aluminium and nickel oxides and chlorides on the alloy surface. It was confirmed by XRD analysis, which indicates the presence of Al_7Cu_4Ni, $Al_7Cu_{23}Ni$, CuO and CuCl compounds.

Acknowledgements

This work was supported by EUREKA Project E! 3704 RSSMA "Rapidly Solidified Shape Memory Alloys" by the Ministry of Science, Education and Sports of the Republic of Croatia.

References

[1] E.A. Ashour, B.G. Ateya, Electrochemical behaviour of a copper–aluminium alloy in concentrated alkaline solutions, Electrochim. Acta 42 (1997) 243–250.
[2] X.Z. Zhou, C.P. Deng, Y.C. Su, Comparative study on the electrochemical performance of the Cu–30Ni and Cu–20Zn–10Ni alloys, J. Alloys Compd. 491 (2010) 92–97.
[3] Lj. Alijnović, S. Gudić, M. Šmith, Inhibition of CuNi10Fe corrosion in seawater by sodium-diethyl-dithiocarbamate: an electrochemical and analytical study, J. Appl. Electrochem. 30 (2000) 973–979.
[4] J. Font, E. Cesari, J. Muntasell, J. Pons, Thermomechanical cycling in Cu–Al–Ni-based melt-spun shape-memory ribbons, Mater. Sci. Eng. A 354 (2003) 207–211.
[5] C. Tatar, R. Zengin, The effects of γ-irradiation on some physical properties of Cu–13.5 wt.%Al–4 wt.%Ni shape memory alloy, Mater. Lett. 59 (2005) 3304–3307.
[6] K. Otsuka, X. Ren, Recent developments in the research of shape memory alloys, Intermetallics 7 (1999) 511–528.
[7] W. Huang, On the selection of shape memory alloys for actuators, Mater. Des. 23 (2002) 11–19.
[8] A. Creuziger, W.C. Crone, Grain boundary fracture in CuAlNi shape memory alloys, Mater. Sci. Eng. A 498 (2008) 404–411.
[9] F. Dagdelen, T. Gokhan, A. Aydogdu, Y. Aydogdu, O. Adigüzel, Effects of thermal treatments on transformation behaviour in shape memory Cu–Al–Ni alloys, Mater. Lett. 57 (2003) 1079–1085.
[10] U. Sari, I. Aksoy, Electron microscopy study of 2H and 18R martensites in Cu–11.92 wt% Al–3.78 wt% Ni shape memory alloy, J. Alloys Compd. 417 (2006) 138–142.
[11] H. Morawiec, J. Lelatko, D. Stróż, M. Gigla, Structure and properties of melt-spun Cu–Al–Ni shape memory alloys, Mater. Sci. Eng. A 273–275 (1999) 708–712.
[12] D.C. Lagoudas, Shape Memory Alloys Modeling and Engineering Applications, Springer, New York, 2008.
[13] A. Subramaniam, Fatigue behavior of copper zinc aluminum shape memory alloys, Master thesis, University of Manitoba, Winnipeg, 1998.
[14] S.S. Rosatto, P.L. Cabot, P.T.A. Sumodjo, A.V. Benedetti, Electrochemical studies of copper–aluminum–silver alloys in 0.5 M H_2SO_4, Electrochim. Acta 46 (2001) 1043–1051.

[15] W.A. Badawy, R.M. El-Sherif, H. Shehata, Electrochemical stability of Cu–10Al–5Ni alloy in chloride–sulfate electrolytes, Electrochim. Acta 54 (2009) 4501–4505.
[16] A.M. Alfantazi, T.M. Ahmed, D. Tromans, Corrosion behavior of copper alloys in chloride media, Mater. Des. 30 (2009) 2425–2430.
[17] A.V. Benedetti, P.T.A. Sumodjo, K. Nobe, P.L. Cabot, W.G. Proud, Electrochemical studies of copper, copper–aluminium and copper–aluminium–silver alloys: impedance results in 0.5 M NaCl, Electrochim. Acta 40 (1995) 2657–2668.
[18] R.F. North, M.J. Pryor, The influence of corrosion product structure on the corrosion rate of Cu–Ni alloys, Corros. Sci. 10 (1970) 297–311.
[19] G. Kear, B.D. Barker, F.C. Walsh, Electrochemical corrosion of unalloyed copper in chloride media––a critical review, Corros. Sci. 46 (2004) 109–135.
[20] S.M. Milić, M.M. Antonijević, S.M. Šerbula, G.D. Bogdanović, Influence of benzotriazole on corrosion behaviour of CuAlNiSi alloy in alkaline medium, Corros. Eng. Sci. Technol. 43 (2008) 30–37.
[21] J.M. Gomez de Salazar, A. Soria, M.I. Barrena, Corrosion behaviour of Cu-based shape memory alloys, diffusion bonded, J. Alloys Compd. 387 (2005) 109–114.
[22] H. Otmačić, J. Telegdi, K. Papp, E. Stupnišek-Lisac, Protective properties of an inhibitor layer formed on copper in neutral chloride solution, J. Appl. Electrochem. 34 (2004) 545–550.
[23] C.I. Elsner, R.C. Salvarezza, A.J. Arvia, The influence of halide ions at submonolayer levels on the formation of oxide layer and electrodissolution of copper in neutral solutions, Electrochim. Acta 33 (1988) 1735–1741.
[24] G. Cicileo, B. Rosales, F. Varela, J. Vilche, Comparative study of organic inhibitors of copper corrosion, Corros. Sci. 41 (1999) 1359–1375.
[25] D. Zhang, L. Gao, G. Zhou, Inhibition of copper corrosion by bis-(1-benzotriazolymethylene)-(2,5-thiadiazoly)-disulfide in chloride media, Appl. Surf. Sci. 225 (2004) 287–293.
[26] A. Srivastava, R. Balasubramaniam, Electrochemical impedance spectroscopy study of surface films formed on copper in aqueous environments, Mater. Corros. 56 (2005) 611–618.
[27] W.A. Badawy, K.M. Ismail, A.M. Fathi, Effect of Ni content on the corrosion behavior of Cu–Ni alloys in neutral chloride solutions, Electrochim. Acta 50 (2005) 3603–3608.
[28] E. Sherif, S.M. Park, Inhibition of copper corrosion in acidic pickling solutions by *N*-phenyl-1 4-phenylenediamine, Electrochim. Acta 51 (2006) 4665–4673.
[29] A.D. Armstrong, Diagnostic criteria for distinguishing between the dissolution–precipitation and the solid state mechanisms of passivation, Corros. Sci. 11 (1971) 693–697.
[30] I.D. Raistrick, J.R. Macdonald, D.R. Franceschetti, in: J.R. Macdonald (Ed.), Impedance Spectroscopy, J. Wiley & Sons, New York, 1987.
[31] J. Hitzig, J. Titz, K. Jüttner, W.J. Lorenz, E. Schmidt, Frequency response analysis of the Ag/Ag^+ system: a partially active electrode approach, Electrochim. Acta 29 (1984) 287–296.
[32] A.E. Bohe, J.R. Vilche, K. Jüttner, W.J. Lorenz, W. Paatsch, Investigations of the semiconductor properties of anodically formed passive layers on Zn and of ZnO single crystals in different aqueous electrolytes by EIS, Electrochim. Acta 34 (1989) 1443–1448.
[33] U. Rammelt, G. Reinhard, On the applicability of a constant phase element (CPE) to the estimation of roughness of solid metal electrodes, Electrochim. Acta 35 (1990) 1045–1049.
[34] Z. Stoynov, Impedance modelling and data processing: structural and parametrical estimation, Electrochim. Acta 35 (1990) 1493–1499.
[35] A. Popova, E. Sokolova, A. Raicheva, M. Christova, AC and DC study of the temperature effect on mild steel corrosion in acid media in the presence of benzimidazole derivatives, Corros. Sci. 45 (2003) 33–58.
[36] D. Kek-Merl, J. Lappalainen, H.L. Tuller, Electrical properties of nanocrystalline CeO2 thin films deposited by in situ pulsed laser deposition, J. Electrochem. Soc. 153 (2006) J15–J20.
[37] G. Lojen, I. Anžel, A. Kneissl, A. Križman, E. Unterweger, B. Kosec, M. Bizjak, Microstructure of rapidly solidified Cu–Al–Ni shape memory alloy ribbons, J. Mater. Process. Technol. 162–163 (2005) 220–229.
[38] C. Deslouis, B. Tribollet, G. Mengoli, M.M. Musiani, Electrochemical behaviour of copper in neutral aerated chloride solution. II. Impedance investigation, J. Appl. Electrochem. 18 (1988) 384–393.